Analytical Calculation of the Magnetic Field in Electrical Machines due to the Current Density in an Airgap Winding

S.R. Holm[1], H. Polinder[1], J.A. Ferreira[1], M.J. Hoeijmakers[1], P. van Gelder[2] and R. Dill[2]

[1] Electrical Power Processing, ITS Faculty, Delft University of Technology
Mekelweg 4, 2628 CD Delft, The Netherlands
phone: +31-15-278-1898 – fax: +31-15-278-2968 – email: S.R.Holm@its.tudelft.nl

[2] Power Electronics & Electromagnetic Conversion, TNO-Prins Maurits Laboratory, Research Group Platform Technology
TNO - Netherlands Organization for Applied Scientific Research
Lange Kleiweg 137, 2280 AA Rijswijk, The Netherlands
phone: +31-15-278-9149 – fax: +31-15-284-3959 – email: dill@pml.tno.nl

***Abstract* – An electrical machine was designed for an energy storage flywheel in a load-levelling system for a city bus. This machine has a slotless stator, and was designed by the use of analytical field calculations. The calculation of the field due to the current distribution in the airgap forms the main contribution of this paper. The results of the analytical field calculations are verified with the finite element method (FEM).**

1. Introduction

The work described in this paper forms part of a research project into the energy storage part of a load-levelling system for city busses and light rail vehicles. The specified stored energy is 7.2 MJ usable with an output power of 200 kW continuous. Fig. 1 shows a block diagram of the electrical system of the city bus. The internal combustion engine turns the shaft of a dc generator. This dc current is processed by a dc-dc converter to drive a traction motor when the vehicle is driven. The flywheel energy storage unit is connected to the dc bus via a bidirectional three-phase ac-dc converter, and can be charged or discharged from this dc bus.

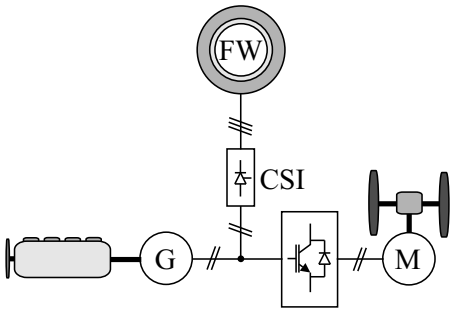

Fig. 1. The electrical system of the city bus.

The energy storage element of the system is a high-speed composite flywheel, into which an external rotor permanent magnet synchronous machine is integrated. (See [1] for a description of such a flywheel machine, in their case for a slotted stator). The effect of stator slotting on stator core and conductor loss was investigated in [2], showing a clear advantage of slotless stators under certain circumstances.

To minimize the stator loss, the electrical machine (of which the geometry is shown in Fig. 2) was therefore designed to have a slotless stator. Analytical field calculations formed the basis of this machine design. This paper describes an extension of the analytical field calculations done in [3], where the field in the flywheel machine due to three different permanent magnet arrays were calculated, and it was shown that the standard permanent magnet array is the best choice in this case. This paper continues on this work, and more specifically, it describes the calculation of the field due to the current in the airgap winding, from which the inductance is calculated. The results of the analytical field calculations are verified with the finite element method (FEM).

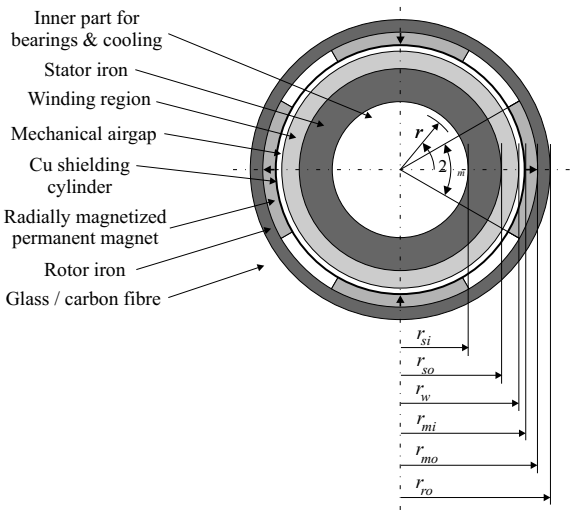

Fig. 2. The electrical machine geometry.

2. Analytical field calculations

A. Previous work by other researchers

As shown in [4], calculating the machine inductance of slotless permanent magnet machines with simple 1D-models is usually inappropriate. These methods may also even be unsuitable for slotted permanent magnet machines with surface mounted magnets [4, 5]. Since accurate prediction of the fields and inductances of the flywheel machine considered in this work is very important, the choice was made to use 2D analytical field calculations for this work.

Calculation of the magnetic field in the airgap of machines with slotted stators due to the stator currents have

been documented in literature: [6], [7] (with improvements in [8]) and [9]. The approach here is to use an equivalent surface current density, located at the stator surface. For a slotless stator, this approach is not valid, and the field due to the current density in the airgap needs to be calculated directly. This has been done in [4] and in this paper. In [4], the results obtained from the 2D-calculation of the field and inductance were compared with 1D-methods, finite element analysis and measurements, showing good agreement. The difference between this paper and [4] is that the current density there is obtained by a single Fourier-series approximation for the current density for the whole winding region. (This was also done in [10]). In this paper, the current density in the three-phase winding of the flywheel machine of Fig. 2 is developed directly from its winding distribution. However, the derivation is kept sufficiently general and transparent so that other winding distributions can be investigated simply by changing the winding factors. The definition of the current density introduced here is also slightly different from that in [4], while the calculation of the inductance is done using a different approach. In [4], the inductance is deduced from the field energy, while in this paper, it is directly calculated from the vector potential.

Strictly speaking, the use of winding factors in multilayer airgap windings is not appropriate, since the flux linkage of the bottom conductors is different from that of the top conductors. However, winding factors have been used in multilayer airgap windings by several researchers: [4], [10] and [11], of which [4] and [10] include experimental validation.

In this paper, the flux linkage is derived as a function of the radius r, so that it can be evaluated at any location inside the winding. For the exterior rotor machine under consideration in this paper, the flux linkage (of the field due to the stator currents) of the outer layer is lower than that of the inner layer. As a first approach, the inductance of the machine is therefore calculated at an r equal to the center of the winding region, where an average flux linkage is located.

B. Motivation for the use of the vector potential

The vector fields **B** and **H** vary with position in a medium. With every such field a potential may be associated where the field relates to the potential and some combination of its positional derivatives. Depending on the nature of the vector field, this potential can either be a scalar potential or a vector potential.

A vector field can either be solenoidal, or irrotational, or both. A vector field **X** is said to be solenoidal if $\nabla \cdot \mathbf{X} = 0$, and irrotational if $\nabla \times \mathbf{X} = \mathbf{0}$. Solenoidal vector fields may be represented by a vector potential, and irrotational vector fields by a scalar potential [12, 13]. The relationships between the potentials associated with magnetic fields and these fields are listed in Table I. In Table I one can see that it is straightforward to obtain the vector field once its associated potential has been obtained.

Ampère's Law:

$$\nabla \times \mathbf{H} = \mathbf{J}, \tag{1}$$

shows that **H** is only irrotational in regions where there is no current density. However, it is possible to use the magnetic scalar potential in regions where a non-zero current density exists by introducing the electric vector potential **T** [13]. This potential is defined by rewriting Ampères Law as $\nabla \times (\mathbf{H} - \mathbf{T}) = \mathbf{0}$, where the electric vector potential **T** is defined implicitly by $\mathbf{J} \equiv \nabla \times \mathbf{T}$, similar to the definition of the magnetic vector potential **A**:

$$\mathbf{B} \equiv \nabla \times \mathbf{A}. \tag{2}$$

As indicated in Table I, by introducing the electric vector potential, the condition for obtaining the magnetic field in all regions therefore changes from $\mathbf{J} = \mathbf{0}$ to $\nabla \cdot \mathbf{J} = \mathbf{0}$, i.e. the current-carrying region must be a perfect conductor.

On the contrary, the magnetic flux density **B** is always solenoidal, for all **J**, due to the law of conservation of magnetic flux:

$$\nabla \cdot \mathbf{B} = 0. \tag{3}$$

The following advantages of using the magnetic vector potential **A** are identified:

- as shown above, finding **A** is a very convenient way to obtain **B** in any region with no constraints on **J**;
- as shown in [6] and [12], in cylindrical coordinates for 2D-fields, the magnetic field lines are simply the equipotential curves of **A**; and
- as shown in [6] and [12], the flux linkage (and consequently inductance and no-load voltage) can be obtained directly from **A**.

The latter statement can be seen from the fact that the flux linkage λ can be written as:

$$\lambda = \iint_S \mathbf{B} \cdot d\mathbf{a} = \iint_S \nabla \times \mathbf{A} \cdot d\mathbf{a} = \oint_C \mathbf{A} \cdot d\mathbf{s}, \tag{4}$$

from (2) and Stokes' integral theorem. The contribution to the contour integral in (4) along curves in a XY-plane is zero [12]. Therefore, the total flux linked by a full-pitch turn at a radius r and angle ϕ is simply [14]:

$$\begin{aligned}\lambda_t(r,\phi) &= l_s \left[A_z(r,\phi) - A_z\left(r, \phi + \tfrac{\pi}{p}\right)\right] \\ &= 2 l_s A_z(r,\phi),\end{aligned} \tag{5}$$

where the periodic boundary condition $A_z(r,\phi) = -A_z\left(r, \phi + \frac{\pi}{p}\right)$ is assumed to be valid.

Due to the reasons listed above, in this paper the vector potential is chosen for the solution of the magnetic field due to **J** (and consequently the calculation of the inductance).

C. Obtaining the magnetic field due to the current density by use of the magnetic vector potential

Poisson's equation has been derived in [3], and this derivation will not be repeated here. It is given by:

$$-\nabla^2 \mathbf{A} = \mu \mathbf{J} + \nabla \times \mathbf{B}_{rem} \tag{6}$$

TABLE I
RELATIONSHIP BETWEEN POTENTIALS AND MAGNETIC FIELDS.

Vector field	Associated scalar potential	Associated vector potential	Relationship	Condition
$\mathbf{H}$	V_m	–	$\mathbf{H} = -\nabla V_m$	if $\mathbf{J} = \mathbf{0}$
$\mathbf{H} - \mathbf{T}$	V_m	–	$\mathbf{H} - \mathbf{T} = -\nabla V_m$	if $\nabla \cdot \mathbf{J} = 0$
$\mathbf{B}$	–	$\mathbf{A}$	$\mathbf{B} = \nabla \times \mathbf{A}$	none

The field due to the magnets, solved in [3], is obtained by setting $\mathbf{J} = \mathbf{0}$ in (6), and the field due to the currents is obtained by setting $\mathbf{B}_{rem} = \mathbf{0}$.

In this paper, Poisson's equation (6) is solved in cylindrical coordinates for two-dimensional fields with $\mathbf{B}_{rem} = \mathbf{0}$. The r- and ϕ-components of the vector potential are thus neglected, and it is assumed that the z-component is independent of z. Thus $\mathbf{A} = A_z(r,\phi)\hat{\mathbf{i}}_z$, and from (2) it follows that $\mathbf{B} = B_r(r,\phi)\hat{\mathbf{i}}_r + B_\phi(r,\phi)\hat{\mathbf{i}}_\phi$. This simplifies the equations a great deal, and one can write Poisson's equation for the z-component of $\mathbf{A}$ as:

$$\frac{\partial^2 A_z}{\partial r^2} + \frac{1}{r^2}\frac{\partial^2 A_z}{\partial \phi^2} + \frac{1}{r}\frac{\partial A_z}{\partial r} = -\mu_0 J_z, \tag{7}$$

where μ_0 is the permeability of free space.

From (2), the relationship between the magnetic vector potential and the flux density is now given by:

$$B_r\hat{\mathbf{i}}_r + B_\phi\hat{\mathbf{i}}_\phi = \frac{1}{r}\frac{\partial A_z}{\partial \phi}\hat{\mathbf{i}}_r - \frac{\partial A_z}{\partial r}\hat{\mathbf{i}}_\phi. \tag{8}$$

3. Solution to Poisson's equation

A. General solution to Poisson's equation

The general solution to Poisson's equation (7) in a region ν can be written as:

$$\begin{aligned} A_z^\nu(r,\phi,t) &= \sum_{k=1}^{\infty} \widehat{A}_{z,k}^\nu(r)\left[\sin(kp\phi)\tilde{i}_{sa}(t)\right. \\ &\left. + \sin\left[kp\left(\phi - \tfrac{2\pi}{3p}\right)\right]\tilde{i}_{sb}(t) + \sin\left[kp\left(\phi - \tfrac{4\pi}{3p}\right)\right]\tilde{i}_{sc}(t)\right]; \\ \widehat{A}_{z,k}^\nu(r) &= C_k^\nu\left(\frac{r}{r_\nu}\right)^{-kp} + D_k^\nu\left(\frac{r}{r_\nu}\right)^{kp} + \widehat{A}_{part,z,k}^\nu(r), \end{aligned} \tag{9}$$

where $\widehat{A}_{part,z,k}^\nu(r)$ is a particular solution. It is zero in all the machine regions except in the winding region. The constants C_k^ν and D_k^ν are obtained from the boundary conditions:

$$H_\phi^\nu(r_\nu,\phi) - H_\phi^{\nu+1}(r_\nu,\phi) = -K_\phi^\nu(r_\nu,\phi), \tag{10}$$

and

$$B_r^\nu(r_\nu,\phi) - B_r^{\nu+1}(r_\nu,\phi) = 0. \tag{11}$$

In this paper, the surface current density $K_\phi^\nu(r_\nu,\phi)$ in (10) is zero for all regions (for all ν).

The particular solution in (9) depends on the current density J_z. In order to find it, the winding distribution is needed first.

B. Obtaining the winding distribution

The flywheel machine of Fig. 2 has a double-layer airgap winding placed in a slotted structure made of synthetic, non-metallic material for mechanical strength. The stator has $s = 2mpq = 36$ slots in total, with: $m = 3$ phases, $p = 2$ pole pairs and $q = 3$ slots per pole per phase. The second layer is short-pitched by one slot. Fig. 3 shows a linear depiction of the winding distribution of phase a.

In general, for the winding distribution of a three-phase winding (the number of conductors per radian [15]), we write:

$$\begin{aligned} n_{sa}(\phi) &= \sum_{k=1,3,5,\ldots}^{\infty} \widehat{n}_{s,k}\sin(kp\phi), \\ n_{sb}(\phi) &= \sum_{k=1,3,5,\ldots}^{\infty} \widehat{n}_{s,k}\sin\left[kp\left(\phi - \tfrac{2\pi}{3p}\right)\right], \\ n_{sc}(\phi) &= \sum_{k=1,3,5,\ldots}^{\infty} \widehat{n}_{s,k}\sin\left[kp\left(\phi - \tfrac{4\pi}{3p}\right)\right], \end{aligned} \tag{12}$$

where the Fourier-coefficient $\widehat{n}_{s,k}$ is twice the number of turns of the k-th space harmonic $N_{s,k}$ [14], or:

$$\widehat{n}_{s,k} = \tfrac{1}{2}N_{s,k}. \tag{13}$$

The number of turns of the k-th space harmonic is related to the real number of turns N by:

$$N_{s,k} = \tfrac{4}{\pi}\,k_{w,k}\,N\sin\left(\tfrac{1}{2}\,k\pi\right) \tag{14}$$

where $k_{w,k}$ is the winding factor for the k-th space harmonic of the actual winding.

The winding factor is the product of different contributions:

$$k_{w,k} = k_{w,slot,k}\;k_{w,dist,k}\;k_{w,pitch,k}\;k_{w,skew,k}. \tag{15}$$

In the flywheel machine discussed here with the winding distribution shown in Fig. 3, all winding factors are used except the skew factor.

C. Obtaining the current density from the winding distribution

The number of turns per radian for phases a, b and c is given by (12). If this is divided by the outer radius of the winding (r_w), the number of turns per meter at that radius is obtained

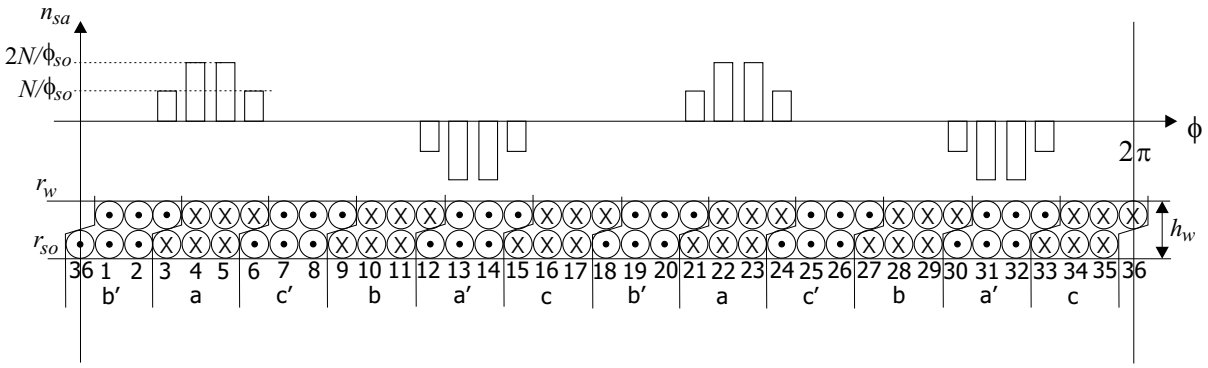

Fig. 3. A linear depiction of the winding distribution of the flywheel machine.

[14]. This result can then be divided by the winding height h_w, defined by:

$$h_w \equiv r_w - r_{so}, \tag{16}$$

to obtain the number of turns per square meter for a winding with outer radius r_w. Multiplying this result with the current in the phase under consideration, one obtains the current per square meter around the circumference, i.e. the current density:

$$J_{sx}(\phi,t) = \frac{n_{sx}(\phi)}{h_w r_w}\, i_{sx}(t) \quad [\mathrm{A/m^2}], \tag{17}$$

where $i_{sx}(t)$ is the current in phase $x = a, b, c$, and $n_{sx}(\phi)$ is given by (12).

The total current density can be obtained by adding the current density of the three phases together. For the k-th space harmonic this becomes,

$$J_{s,k}(\phi,t) = J_{sa,k}(\phi,t) + J_{sb,k}(\phi,t) + J_{sc,k}(\phi,t), \tag{18}$$

where, from equation (17):

$$J_{sx,k}(\phi,t) = \frac{n_{sx,k}(\phi)}{h_w r_w}\, i_{sx}(t); \quad x = a, b, c, \tag{19}$$

and, from equation (12):

$$\begin{aligned} n_{sa,k}(\phi) &= \widehat{n}_{s,k}\sin(kp\phi), \\ n_{sb,k}(\phi) &= \widehat{n}_{s,k}\sin\left[kp\left(\phi - \tfrac{2\pi}{3p}\right)\right], \\ n_{sc,k}(\phi) &= \widehat{n}_{s,k}\sin\left[kp\left(\phi - \tfrac{4\pi}{3p}\right)\right]. \end{aligned} \tag{20}$$

By use of (19) and (20), equation (18) can be written as:

$$\begin{aligned} J_{s,k}(\phi,t) = \frac{\widehat{n}_{s,k}\,\hat{i}_s}{h_w r_w} \; &\left[\sin(kp\phi)\tilde{i}_{sa}(t)\right. \\ &\left. + \sin\left[kp\left(\phi - \tfrac{2\pi}{3p}\right)\right]\tilde{i}_{sb}(t) + \sin\left[kp\left(\phi - \tfrac{4\pi}{3p}\right)\right]\tilde{i}_{sc}(t)\right], \end{aligned} \tag{21}$$

where the normalized currents:

$$\tilde{i}_{sx}(t) \equiv i_{sx}(t)/\hat{i}_s; \quad x = a, b, c, \tag{22}$$

have been introduced, and $\hat{i}_s$ is the peak value of the (balanced) stator currents.

Furthermore, by defining:

$$\widehat{J}_{s,k} \equiv \frac{\widehat{n}_{s,k}\hat{i}_s}{h_w r_w}, \tag{23}$$

equation (21) can be rewritten as:

$$\begin{aligned} J_{s,k}(\phi,t) = \widehat{J}_{s,k} \; &\left[\sin(kp\phi)\tilde{i}_{sa}(t)\right. \\ &\left. + \sin\left[kp\left(\phi - \tfrac{2\pi}{3p}\right)\right]\tilde{i}_{sb}(t) + \sin\left[kp\left(\phi - \tfrac{4\pi}{3p}\right)\right]\tilde{i}_{sc}(t)\right]. \end{aligned} \tag{24}$$

D. Solution of the vector potential and magnetic field

The flywheel machine regions shown in Fig. 2 are numbered from the inside: $\nu = 1$: stator iron; $\nu = 2$: winding region; $\nu = 3$: mechanical airgap & permanent magnet region; $\nu = 4$: rotor iron; and $\nu = 5$: glass fibre.

For a current density for which the k-th space harmonic is given by (24), the particular solution in the copper region ($\nu = 2$) is now time-dependent:

$$\begin{aligned} A^2_{part,z}(r,\phi,t) = \sum_{k=1}^{\infty} \widehat{A}^2_{part,z,k}(r) \; &\left[\sin(kp\phi)\tilde{i}_{sa}(t)\right. \\ &\left. + \sin\left[kp\left(\phi - \tfrac{2\pi}{3p}\right)\right]\tilde{i}_{sb}(t) + \sin\left[kp\left(\phi - \tfrac{4\pi}{3p}\right)\right]\tilde{i}_{sc}(t)\right]; \end{aligned}$$

$$\widehat{A}^2_{part,z,k}(r) = \begin{cases} \frac{\mu_0 \widehat{J}_{s,k} r^2}{(kp)^2 - 4} & \text{if } kp \neq 2 \\ \frac{1}{4}\mu_0 \widehat{J}_{s,k} r^2\left(-\ln(r) + \frac{1}{4}\right) & \text{if } kp = 2 \end{cases} \tag{25}$$

The vector potential was solved in the five regions in the machine, but only the expressions for the winding region ($\nu = 2$) and the mechanical airgap & magnet region ($\nu = 3$) is listed in the paper, in Appendix A.

E. Calculation of the machine inductance from the vector potential

The total flux linked by a full-pitch turn at a radius r and angle ϕ was shown to be given by (5). From this, the flux linked with phase a of an airgap winding with arbitrary dis-

tribution $n_{sa}(\phi)$ at any radius r is:

$$\lambda_{sa}(r) = p \int_0^{\pi/p} n_{sa}(\phi)\lambda_t(r,\phi)d\phi = 2p\, l_s \int_0^{\pi/p} n_{sa}(\phi)A_z(r,\phi)d\phi, \quad (26)$$

from equation (5).

The flux linkage due to the magnetic field of the stator currents can be written as:

$$\overrightarrow{\lambda}_{ss} = \sum_{k=1,3,5,\ldots}^{\infty} \mathbf{L_{ss,k}} \overrightarrow{i_s}, \quad (27)$$

where

$$\mathbf{L_{ss,k}} = L_{ss,k} \begin{bmatrix} 1 & \cos\left(\frac{2k\pi}{3}\right) & \cos\left(\frac{2k\pi}{3}\right) \\ \cos\left(\frac{2k\pi}{3}\right) & 1 & \cos\left(\frac{2k\pi}{3}\right) \\ \cos\left(\frac{2k\pi}{3}\right) & \cos\left(\frac{2k\pi}{3}\right) & 1 \end{bmatrix} \quad (28)$$

and

$$\overrightarrow{\lambda}_{ss} = \begin{bmatrix} \lambda_{sa} \\ \lambda_{sb} \\ \lambda_{sc} \end{bmatrix}; \qquad \overrightarrow{i_s} = \begin{bmatrix} i_{sa} \\ i_{sb} \\ i_{sc} \end{bmatrix} \quad (29)$$

The inductance-term $L_{ss,k}$ in (28) is given directly from the vector potential from (9), (12), (26), (27), (28) and (29) as:

$$L_{ss,k} = \pi l_s \widehat{n}_{s,k} \widehat{A}^2_{z,k}(r_{avg}). \quad (30)$$

The synchronous per-phase inductance is calculated from (30) by taking only the fundamental harmonic into account:

$$L_s = \tfrac{3}{2} L_{ss,1}. \quad (31)$$

For the flywheel machine, this inductance is calculated as 47.6 μH.

The leakage inductance is given by an expression similar to (28), although a closed-form expression for the leakage inductance has not been derived. In standard slotted machines, the leakage inductance $L_{s\sigma}$ consists of the airgap leakage, end-winding leakage, and slot leakage. In expression (30) derived above for the inductance $L_{ss,k}$, the airgap leakage and slot leakage is also included.

4. Results

Fig. 4 shows a field plot due to the current flowing in an airgap winding of the external rotor permanent magnet synchronous machine of Fig. 2. In this figure, the time t was chosen such that $i_a = 0$ and $i_b = -i_c$.

Fig. 5 shows a comparison of the radial component of the magnetic flux density calculated with the FEM and the analytical method in the winding region for the machine of Fig. 2. As can be seen, there is good correlation except at the last current-carrying slot, where the FEM-calculation exhibits peculiar behavior. This is due to the modelling of the airgap winding in the FEM package, and is under investigation.

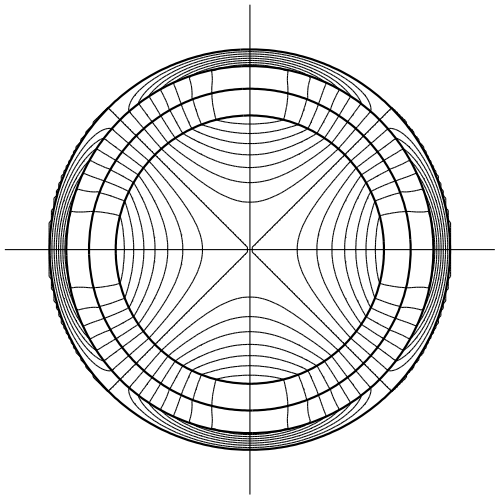

Fig. 4. Magnetic field lines in the external rotor permanent magnet synchronous machine of Fig. 2 due to the current flowing in an airgap winding.

5. Conclusion

In this paper, an external rotor permanent magnet synchronous machine applied in an energy storage flywheel was described. Specifically, the calculation of the magnetic field in this machine due to the stator currents flowing in its airgap winding was discussed. It was shown that the vector potential **A** is the preferred potential to obtain the field variables **B** and **H** with no constraints on **J**. A closed-form analytical expression for the vector potential and the flux density (not listed) was derived directly from the three-phase stator winding distribution. It was shown that the flux linkage of the airgap winding, and consequently the inductance, may be obtained directly from **A**. The results of the flux density in the winding as calculated with this method was compared with the FEM, and good correlation was achieved.

Acknowledgement

The work of T. Huijser of TNO-PML on the finite element calculations is gratefully acknowledged.

Appendices

A The vector potential in the regions $\nu = 2$ and 3

The vector potential is given by:

$$A_z^{\nu}(r,\phi,t) = \sum_{k=1,3,5,\ldots}^{\infty} \widehat{A}^{\nu}_{z,k}(r) \left[\sin(kp\phi)\tilde{i}_{sa}(t) + \sin\left[kp\left(\phi - \tfrac{2\pi}{3p}\right)\right]\tilde{i}_{sb}(t) + \sin\left[kp\left(\phi - \tfrac{4\pi}{3p}\right)\right]\tilde{i}_{sc}(t)\right];$$

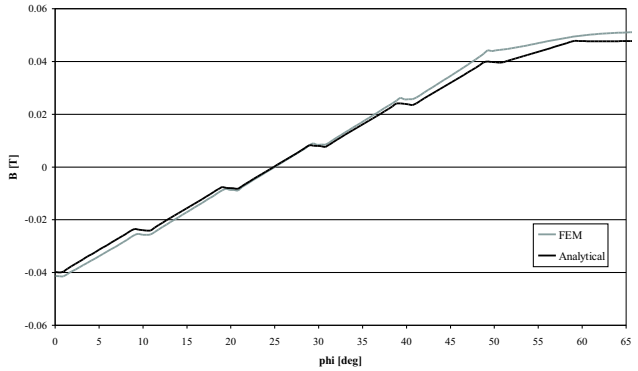

Fig. 5. Comparison of the radial component of the magnetic flux density calculated with the FEM and the analytical method in the winding region for the machine of Fig. 2.

where $\nu = 2$ and 3, and:

$$\widehat{A}^{2}_{z,k}(r) =$$

$$\begin{cases} -\frac{1}{2}\mu_0 \widehat{J}_{s,k} \left\{ \left[\frac{-(2+kp)r_w^2 \left(\frac{r_{so}}{r_w}\right)^{2kp} - (2-kp)r_w^2 \left(\frac{r_{so}}{r_{mo}}\right)^{2kp}}{kp\left[(kp)^2-4\right]\left[\left(\frac{r_{so}}{r_{mo}}\right)^{2kp}-1\right]} + \frac{4r_{so}^2\left(\frac{r_{so}}{r_w}\right)^{kp}}{kp\left[(kp)^2-4\right]\left[\left(\frac{r_{so}}{r_{mo}}\right)^{2kp}-1\right]} \right] \left(\frac{r}{r_w}\right)^{-kp} \right. \\ \left. + \left[\frac{-(2+kp)r_w^2 - (2-kp)r_w^2 \left(\frac{r_w}{r_{mo}}\right)^{2kp} + 4r_{so}^2 \left(\frac{r_{so}r_w}{r_{mo}^2}\right)^{kp}}{kp\left[(kp)^2-4\right]\left[\left(\frac{r_{so}}{r_{mo}}\right)^{2kp}-1\right]} \right] \left(\frac{r}{r_w}\right)^{kp} \right\} \\ \quad + \frac{\mu_0 \widehat{J}_{s,k} r^2}{(kp)^2-4} \qquad \text{if } kp \neq 2 \\ -\frac{1}{16}\,\mu_0 \widehat{J}_{s,k} \left\{ \left[\frac{r_{so}^4\left[r_w^4 + 4r_{mo}^4 \ln(r_w) - 4r_{mo}^4 \ln(r_{so}) - r_{mo}^4\right]}{r_w^2\left[r_{so}^4 - r_{mo}^4\right]} \right] \left(\frac{r}{r_w}\right)^{-2} \right. \\ \left. \left[\frac{r_w^2\left[r_w^4 + 4r_{mo}^4 \ln(r_w) - 4r_{so}^4 \ln(r_{so}) - r_{so}^4\right]}{r_{so}^4 - r_{mo}^4} \right] \left(\frac{r}{r_w}\right)^{2} \right\} \\ \quad + \frac{1}{4}\mu_0 \widehat{J}_{s,k} r^2 \left(-\ln(r) + \frac{1}{4}\right) \qquad \text{if } kp = 2 \end{cases}$$

and:

$$\widehat{A}^{3}_{z,k}(r) =$$

$$\begin{cases} \frac{1}{2}\,\mu_0 \widehat{J}_{s,k} \left[\frac{(2-kp)r_w^2\left(\frac{r_w}{r_{mo}}\right)^{kp} + (2+kp)r_w^2\left(\frac{r_{so}^2}{r_w r_{mo}}\right)^{kp} - 4r_{so}^2\left(\frac{r_{so}}{r_{mo}}\right)^{kp}}{kp\left[(kp)^2-4\right]\left[\left(\frac{r_{so}}{r_{mo}}\right)^{2kp}-1\right]} \right] \\ \quad \cdot \left[\left(\frac{r}{r_{mo}}\right)^{-kp} + \left(\frac{r}{r_{mo}}\right)^{kp} \right] \qquad \text{if } kp \neq 2 \\ -\frac{1}{16}\,\mu_0 \widehat{J}_{s,k} \left[\frac{r_{mo}^2\left[r_w^4 + 4r_{so}^4 \ln(r_w) - 4r_{so}^4 \ln(r_{so}) - r_{so}^4\right]}{r_{so}^4 - r_{mo}^4} \right] \\ \quad \cdot \left[\left(\frac{r}{r_{mo}}\right)^{-2} + \left(\frac{r}{r_{mo}}\right)^{2} \right] \qquad \text{if } kp = 2 \end{cases}$$

References

[1] W. Vetter, A. Colotti and K. Reichert, "A new Motor/Generator for Flywheel Applications," *Proc. International Conference on Electrical Machines (ICEM 1996)*, pp. 348–352.

[2] A.A. Arkadan and R. Vyas and J.G. Vaidya and M.J. Sha, "Effect of Toothless Stator Design on Core and Stator Conductors Eddy Current Losses in Permanent Magnet Generators," *IEEE Transactions on Energy Conversion*, Vol. 7, No. 1, March 1992.

[3] S.R. Holm, H. Polinder, J.A. Ferreira, P. van Gelder and R. Dill, "Comparison of Three Permanent Magnet Structures with respect to Torque Production by means of Analytical Field Calculations," *Proc. International Power Electronics, Machines and Drives Conference (PEMD 2002)*, pp. 409–414.

[4] K. Atallah, Z.Q. Zhu, D. Howe and T.S. Birch, "Armature Reaction Field and Winding Inductances of Slotless Permanent-Magnet Brushless Machines," *IEEE Transactions on Magnetics*, Vol. 34, No. 5, pp. 3737–3744, September 1998.

[5] Z.Q. Zhu, D. Howe and T.S. Birch, "Calculation of winding inductances of brushless motors with surface-mounted permanent magnets," *Proc. International Conference on Electrical Machines (ICEM 1994)*, pp. 327–332.

[6] H. Polinder and M.J. Hoeijmakers, "Analytic Calculation of the Magnetic Field in PM Machines," *Proc. 32nd IEEE Industry Applications Society Conference (IAS 1997)*, Vol.1, pp. 35–41.

[7] Z.Q. Zhu and D. Howe, "Instantaneous Magnetic Field Distribution in Brushless Permanent Magnet DC Motors, Part II: Armature-Reaction Field," *IEEE Transactions on Magnetics*, Vol. 29, No. 1, pp. 136–142, January 1993.

[8] Z.Q. Zhu, D. Howe and C.C. Chan, "Improved Analytical Model for Predicting the Magnetic Field Distribution in Brushless Permanent-Magnet Machines," *IEEE Transactions on Magnetics*, Vol. 38, No. 1, pp. 229–238, January 2002.

[9] A. Hughes and T.J.E. Miller, "Analysis of Fields and Inductances in Air-Cored and Iron-Cored Synchronous Machines," *Proceedings of the IEE*, Vol. 124, No. 2, pp. 121–126, February 1977.

[10] K. Sridhar, "Electromagmetic Models for PM Synchronous Motor Drives," *Proc. Tenth Annual Applied Power Electronics Conference and Exposition (APEC 1995)*, pp. 367–377.

[11] Y. Chen, J. Shen and Z. Fang, "Topology and Preliminary Design of Slotless Brushless DC Motor," *Proc. IEEE International Electric Machines and Drives Conference (1997)*, pp. WB2-7.1–WB2-7.3.

[12] H.A. Haus and J.R. Melcher, *Electromagnetic Fields and Energy*, Prentice-Hall, Inc., London (1989).

[13] K. Hameyer and R. Belmans, *Numerical Modelling and Design of Electrical Machines and Devices*, WIT Press, Southampton (1999).

[14] H. Polinder, *On the losses in a high-speed permanent magnet generator with rectifier*, PhD-thesis, Faculty ITS, Delft University of Technology, June 1998.

[15] G.R. Slemon, *Electric Machines and Drives*, Addison-Wesley, Reading, Massachusetts (1992).